Nanowire-Based All-Oxide Solar Cells

Benjamin D. Yuhas and Peidong Yang*

*Department of Chemistry, University of California, Berkeley, and Materials Sciences Division,
Lawrence Berkeley National Laboratory, Berkeley, California 94720*

Received December 7, 2008; E-mail: p_yang@berkeley.edu

Abstract: We present an all-oxide solar cell fabricated from vertically oriented zinc oxide nanowires and cuprous oxide nanoparticles. Our solar cell consists of vertically oriented n-type zinc oxide nanowires, surrounded by a film constructed from p-type cuprous oxide nanoparticles. Our solution-based synthesis of inexpensive and environmentally benign oxide materials in a solar cell would allow for the facile production of large-scale photovoltaic devices. We found that the solar cell performance is enhanced with the addition of an intermediate oxide insulating layer between the nanowires and the nanoparticles. This observation of the important dependence of the shunt resistance on the photovoltaic performance is widely applicable to any nanowire solar cell constructed with the nanowire array in direct contact with one electrode.

Introduction

Solar energy production is fast becoming a vital source of renewable energy being developed as an alternative to traditional fossil fuel-based sources of power. One of the primary challenges to the full-scale implementation of solar energy remains the expensive cost associated with the construction of photovoltaic modules and certain toxic elements in some thin film solar cells. The principal photovoltaic (PV) material on the market today is silicon, and although silicon-based solar cells are comprised of a very abundant element, their large-scale production is hampered by the high cost of processing and refining, which sets the average electricity cost from a silicon solar cell well above that which comes from coal- or gas-burning power plants.[1,2] Although there are solar cells reported with very high efficiencies[3−5] (>25%), these cells are all constructed in a laboratory-scale setting, often requiring rare or expensive materials and/or methods. If a material is truly to become a marketable option for the photovoltaic industry, some consideration must be given to the expense of its synthesis, manufacture, processing, and construction into a device, in addition to its ultimate PV efficiency.

Generally speaking, materials selection for future photovoltaics should satisfy several important criteria. The materials should be comprised of abundant and inexpensive elements. The materials should be environmentally benign to avoid any issues of potential environmental contamination. And importantly for any potential PV application, the materials must have an optimal band gap to maximize solar absorption such that the resulting solar cell would have a marketable energy conversion efficiency.

Among the inorganic materials proposed as a PV alternative to silicon, cuprous oxide (Cu_2O) is one of the most extensively studied,[6] with investigations stretching back more than 20 years. As-made Cu_2O is a p-type semiconductor with a band gap of 2.0 eV, which allows for good solar spectral absorption. The abundance and nontoxicity of copper, as well as the long-term stability associated with oxides, allows for the possibility of constructing durable, long-lasting solar cells with Cu_2O as the active light-absorbing component. There are several examples of Cu_2O-based PV devices reported in the literature, often prepared by using low-cost, solution-based methods.[7−10] However, nearly all of these devices were either bulk or thin-film bilayer cells, and these types of cells suffer from the fact that the optimal material length scales for optical absorption and carrier extraction are contrary to one another. A thicker film will absorb more sunlight, but only the excitons created near the active interface will be effectively split and harvested into an external circuit.

Nanowire-based solar cells have been reported to possess inherent advantages over traditional bilayer devices.[11−15] By separating the optimal length scales for light absorption and exciton diffusion, it is possible to create a device with a relatively thick absorbing layer (for full solar spectral absorption), yet small interwire spacing (for short exciton diffusion).

(1) Shah, A.; Torres, P.; Tscharner, R.; Wyrsch, N.; Keppner, H. *Science* **1999**, *285*, 692.
(2) Green, M. A. *Solar Cells*; Prentice-Hall, Inc.: Englewood Cliffs, NJ, 1982.
(3) King, R. R.; Law, D. C.; Edmondson, K. M.; Fetzer, C. M.; Kinsey, G. S.; Yoon, H.; Sherif, R. A.; Karam, N. H. *Appl. Phys. Lett.* **2007**, *90*, 183516.
(4) Geisz, J.; Kurtz, S; Wanlass, M. W.; Ward, J. S.; Duda, A; Friedman, D. J.; Olson, J. M.; McMahon, W. E.; Moriarty, T. E.; Kiehl, J. T. *Appl. Phys. Lett.* **2007**, *91*, 023502.
(5) Zhao, J.; Wang, A.; Green, M. A. *Prog. Photovoltaics* **1999**, *7*, 471.

(6) Rai, B. P. *Solar Cells* **1988**, *25*, 265.
(7) Minami, T.; Miyata, T.; Ihara, K.; Minamino, Y.; Satoshi, T. *Thin Solid Films* **2006**, *494*, 47.
(8) Akimoto, K.; Ishizuka, S.; Yanagita, M.; Nawa, Y.; Paul, G. K.; Sakurai, T. *Solar Energy* **2006**, *80*, 715.
(9) Katayama, J.; Ito, K.; Matsuoka, M.; Tamaki, J. *J. Appl. Electrochem.* **2004**, *34*, 687.
(10) Izaki, M.; Mizuno, K.; Shinagawa, T.; Inaba, M.; Tasaka, A. *J. Electrochem. Soc.* **2006**, *153*, C668.
(11) Kayes, B. M.; Atwater, H. A.; Lewis, N. S. *J. Appl. Phys.* **2005**, *97*, 114302.
(12) Garnett, E. C.; Yang, P. *J. Am. Chem. Soc.* **2008**, *130*, 9224.
(13) Tian, B.; Zheng, X.; Kempa, T. J.; Fang, Y.; Yu, N.; Yu, G.; Huang, J.; Lieber, C. M. *Nature* **2007**, *449*, 885.
(14) Zhang, Y.; Wang, L.-W.; Mascarenhas, A. *Nano Lett.* **2007**, *7*, 1264.
(15) Law, M.; Greene, L. E.; Johnson, J. C.; Saykally, R.; Yang, P. *Nat. Mater.* **2005**, *4*, 455.

In addition, oriented nanowire arrays have been shown to possess excellent charge transport (and therefore charge collection) characteristics in photovoltaic devices.[15−18]

In this article, we present a novel solar cell design that combines the ideal geometry of a nanowire-based solar cell with the concept of using environmentally friendly, inexpensive, and durable semiconducting PV components. Our solar cell consists of vertically oriented n-type zinc oxide nanowires, surrounded by a film constructed from p-type cuprous oxide nanoparticles. All of the semiconductor synthesis is done in the solution phase, which could allow for facile scaling up of the PV modules. We present results on the PV performance, as well as results on the chemistry of the Cu_2O nanoparticles, and discuss their importance and relevance to other nanoscale PV systems.

Experimental Section

Chemicals. Except where noted, all chemicals were purchased from Sigma-Aldrich, Inc., and used without further purification.

ZnO Nanowires. The ZnO NW arrays were prepared using a synthesis described previously.[19] Briefly, a 5 mM solution of zinc acetate dihydrate in absolute ethanol was prepared. Two drops of this solution were placed onto an indium tin oxide (ITO) coated glass substrate (Thin Film Devices, ∼40−50 Ω/square). The substrate was then rinsed with absolute ethanol and blown dry with nitrogen. The dropcasting, rinsing, and drying were repeated four times per substrate. The substrates were then annealed in air at 350 °C for 30 min, converting the $Zn(OAc)_2$ into ZnO, and then cooled to room temperature. This process was then repeated a second time to ensure a conformal layer of ZnO.

The nanowires were then grown by placing the seeded substrate in an aqueous solution containing 25 mM zinc nitrate hexahydrate, 25 mM hexamethylenetetraamine, and 5 mM polyethyleneimine at 90 °C. The substrate was suspended upside-down to prevent any larger ZnO aggregates from accumulating on the surface. Typical growth times ranged from 30 to 60 min, yielding wires that averaged 400−1000 nm in length and 30−50 nm in diameter. After the growth, the nanowire arrays were rinsed thoroughly with deionized water and then annealed at 400 °C for 30 min to remove any residual organics on the nanowire surface.

Cu_2O Nanoparticles. The Cu_2O nanoparticles (NPs) were prepared after the method of Yin et al.[20] A solution of copper(I) acetate (0.5 g), trioctylamine (15 mL), and oleic acid (Alfa Aesar, 99%, 4 mL) was flushed with nitrogen and then rapidly heated to 180 °C under a nitrogen flow. The solution was maintained at this temperature for 1 h, which then was quickly increased to 270 °C and held for one additional hour, ultimately producing a burgundy colloidal solution, which contains metallic copper nanoparticles. The solution was cooled to room temperature, at which point absolute ethanol was added to precipitate the nanoparticles. The supernatant was removed, and the nanoparticles were redispersed in hexane and then exposed to air. After 12 h, the burgundy solution turned to deep green, indicating the oxidation of the copper nanoparticles into Cu_2O. The Cu_2O nanoparticles underwent further cleaning by repeated precipitation with ethanol. Finally, the nanoparticles were dispersed in toluene for dropcasting onto the ZnO nanowire arrays.

Cu_2O Film Deposition. 100 μL of Cu_2O nanoparticles, dispersed in toluene, were dropcast onto the ZnO nanowire arrays. The arrays were gently heated (∼50 °C) under vacuum while the droplet was

still present to improve the particle filling and the film homogeneity. Then, the films were annealed at temperatures ranging from 200 to 400 °C under reduced pressure (P = 5 Torr, 10% O_2 in argon) or 1 atm of argon for 1 h and then cooled to room temperature. The film thickness was tracked via optical absorption, and the process was repeated to obtain films of the desired thickness.

Solar Cell Fabrication and Testing. A small section of the Cu_2O film and the ZnO NW array was removed with 1 M HCl to allow for the placement of a metal contact on the ITO. Eight Au or Al contact regions (area = 0.03 cm²) were placed via thermal evaporation through a patterned shadow mask under high vacuum (<10⁻⁶ Torr). Current−voltage measurements were performed in the dark and under AM 1.5 and 1 Sun illumination (Oriel, 300 W Model, 91160), with the incident light coming through the backside of the device.

Structural Characterization. Scanning electron microscopy was done on a JEOL JSM-6340F operating at 5 kV. Transmission electron microscopy was performed on a Philips CM200 FEG operating at 200 kV. X-ray diffraction was done on a Bruker GADDS D-8 diffractometer using Co Kα radiation (λ = 1.79 Å). Hall measurements were performed by preparing an annealed film of Cu_2O NPs on an insulating glass substrate measuring 1 cm × 1 cm. The film was contacted at the corners, and the resistivity was measured in the presence and absence of a 5000 Gauss magnetic field. The carrier concentration, mobility, and resistivity of the Cu_2O film were extracted from these measurements.

Results and Discussion

Properties of the Cu_2O Nanoparticles. Figure 1 displays electron micrographs of both of the active components in our all-oxide solar cell: the ZnO NWs and the Cu_2O NPs. Both components are single-crystalline in nature, and owing to their solution-based synthesis, they can theoretically be scaled up with relative ease. The simplest fabrication of the solar cell is displayed in Figure 2. Here, the ZnO NW arrays were filled with Cu_2O NPs by dropcasting a toluene solution of the NPs onto the NW array. It can be seen that the NPs fully penetrate the interwire spacing in the array. In this device, no annealing was performed; the cross-sectional SEM thus shows the Cu_2O film as a waxy solid, owing to the presence of the organic capping agent oleic acid on the Cu_2O NP surface. $J−V$ measurements conducted on this cell show that solar illumination produces an increase in conductivity under forward bias, but no photovoltage was observed.

Annealing treatments were thus performed in an attempt to both remove the surface ligands and sinter the NPs into a more continuous film, which should improve its carrier mobility. Initially, all annealing treatments were performed under argon. Although the Cu_2O NPs are resistant to oxidation under ambient conditions, a transformation to CuO can occur at elevated temperatures in air. The results of annealing treatments at various temperatures under an argon atmosphere are displayed in Figure 3. Surprisingly, at temperatures greater than 250 °C, we observed the appearance of Cu peaks in the XRD patterns. At higher temperatures, this transformation is profound; annealing at 400 °C under argon produced a film that had a reflective copper sheen after 1 h of annealing. This observation was consistently seen regardless of the starting Cu_2O film thickness, and whether the film was embedded in a ZnO NW array (i.e., part of a solar cell) or deposited onto a bare glass substrate.

The reduction of the Cu_2O film into Cu metal is rather mysterious in nature, particularly in the absence of a clear reducing agent. Disproportionation of the Cu_2O into the metal Cu and the higher oxide CuO is thermodynamically unfavorable

(16) Wu, J.-J.; Chen, G.-R.; Yang, H.-H.; Ku, C.-H.; Lai, J.-Y. *Appl. Phys. Lett.* **2007**, *90*, 213109.

(17) Adachi, M.; Sakamoto, M.; Jiu, J.; Ogata, Y.; Isoda, S. *J. Phys. Chem. B* **2006**, *110*, 15932.

(18) Meng, S.; Ren, J.; Kaxiras, E. *Nano Lett.* **2008**, *8*, 3266.

(19) Greene, L.; Law, M.; Tan, D. H.; Goldberger, J.; Yang, P. *Nano Lett.* **2005**, *5*, 1231.

(20) Yin, M.; Wu, C.-K.; Lou, Y.; Burda, C.; Koberstein, J. T.; Zhu, Y.; O'Brien, S. *J. Am. Chem. Soc.* **2005**, *127*, 9506.
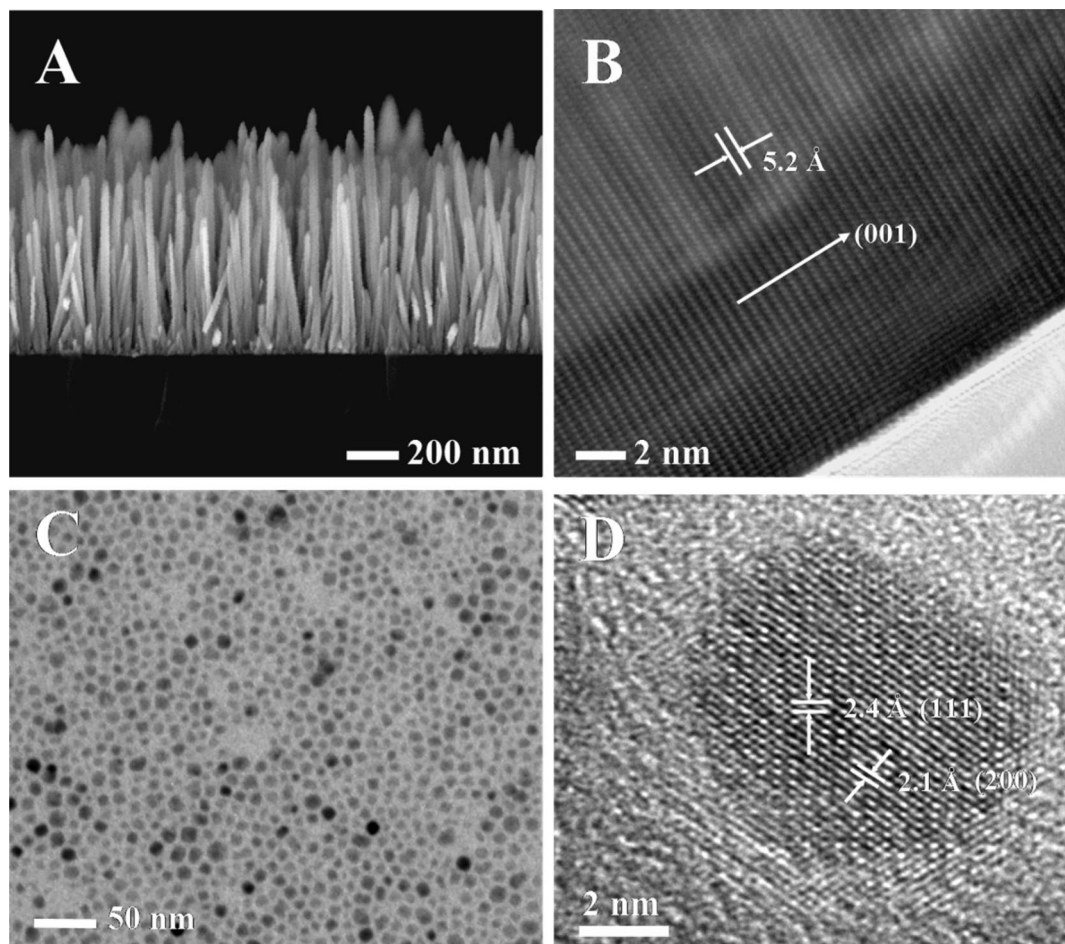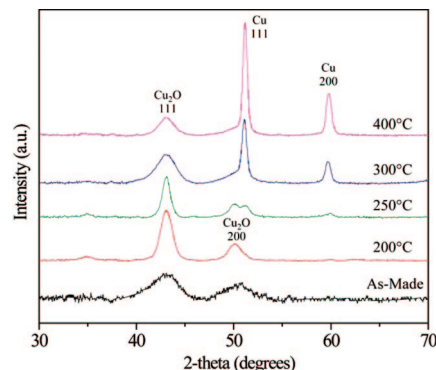
Figure 1. (A) Cross-sectional SEM image of ZnO nanowire array used in solar cells, prior to Cu_2O addition. (B) High-resolution TEM image of an individual ZnO nanowire. (C) Low resolution and (D) high resolution TEM images of Cu_2O nanoparticles.
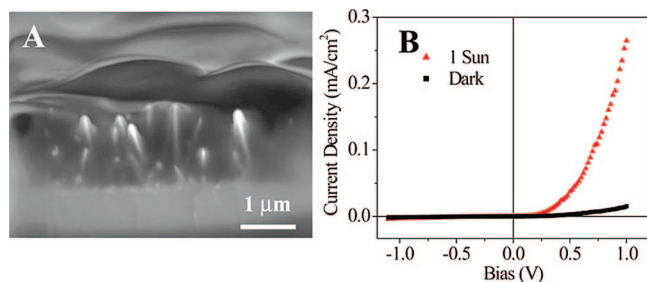
Figure 2. (A) Cross section SEM of a completed ZnO/Cu_2O solar cell, with no Cu_2O annealing performed. (B) The corresponding $J-V$ curve in darkness and under 1 Sun illumination.
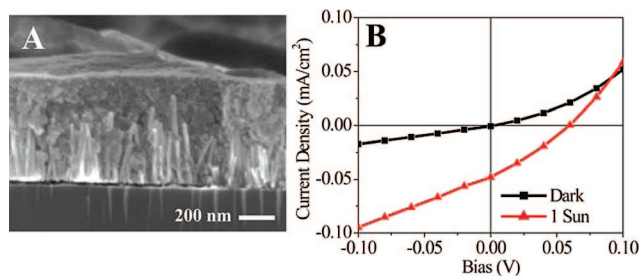

Figure 3. XRD patterns of Cu_2O NPs films on glass, annealed at the noted temperatures under argon. The patterns are vertically offset for clarity.

under standard conditions,[21] and even less so at elevated temperatures. The simple decomposition into copper and oxygen is even less favorable, although it could be argued that it may be driven by the lack of oxygen in the annealing environment, as has been observed in high vacuum annealing studies of Cu_2O thin films.[22]

At the 200 °C annealing condition under argon, no phase transformation of the Cu_2O film was ever observed, although there was significant narrowing of the Bragg peaks in the XRD

pattern. This implies an increased grain size in the Cu_2O film, which will improve the charge transport through the film. A solar cell was constructed using this annealing condition, as shown in Figure 4. The Cu_2O NPs were dropcast and annealed successively; thinner layers of Cu_2O were less susceptible to cracking during annealing. In addition, any textural defects in the film could be filled in with multiple Cu_2O depositions, plus the film thickness could be more easily controlled using this method. The solar performance of the cell is shown in Figure 4B. Although a distinct photovoltage and photocurrent are seen with the cell, they are quite small; the efficiency of this cell is ~0.001%. We thus see that it is vital to increase the grain size

(21) Lide, D. R. , Ed. *CRC Handbook of Chemistry and Physics*, 88th ed.; CRC Press/Taylor and Francis: Boca Raton, FL, 2008.
(22) Lee, S. Y.; Mettlach, N.; Nguyen, N.; Sun, Y. M.; White, J. M. *Appl. Surf. Sci.* **2003**, *206*, 102.

Figure 4. (A) Cross section SEM of a completed ZnO/Cu$_2$O solar cell, with the cell annealed at 200 °C after each application of Cu$_2$O NPs. (B) The corresponding $J-V$ curve in darkness and under AM 1.5 and 1 Sun illumination.
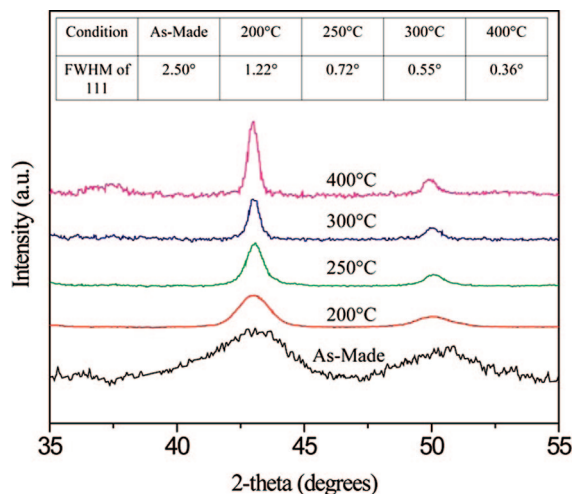
Figure 5. XRD patterns of Cu$_2$O NPs films on glass, annealed at the noted temperatures under 500 mTorr oxygen (total pressure = 5 Torr). The patterns are vertically offset for clarity, and the accompanying table lists the measured fwhm values for the 111 peak at the different annealing temperatures.

in the Cu$_2$O film even further. This could be most easily done by simply raising the annealing temperature. However, the previous issues of phase transformation stated above require a change to the annealing strategy.

To counter the effect of Cu$_2$O reduction, higher temperature anneals (>250 °C) were performed under a reduced partial pressure of oxygen. A 10% O$_2$ in an argon gaseous mixture was used, and the system was placed under vacuum such that the *total* pressure of the annealing tube was 5 Torr (P_{O_2} = 500 mTorr). The XRD patterns of the resulting films are displayed in Figure 5. In all cases, the cuprite phase (Cu$_2$O) was the only one observed. In addition, the elevated annealing temperatures led to a larger reduction in the fwhm of the Bragg peaks. This implies a greatly improved sintering of the Cu$_2$O NPs into a more continuous film, which will be very important for hole transport in the solar cell.

The improvement in the quality of the Cu$_2$O films upon higher temperature annealing is also evident from the charge transport characteristics. Table 1 lists the carrier concentrations, mobilities, and resistivities acquired from Hall measurements performed on Cu$_2$O films prepared on glass. The film composition was confirmed with XRD prior to Hall measurements. All of the films were pure Cu$_2$O, and no metallic conductivity was observed. The beneficial effects from annealing at higher temperatures are seen in lower resistivities as well as moderately increased carrier concentrations. The mobility of the films was rather constant, and all of the films exhibited p-type behavior.

Table 1. Carrier Concentrations, Mobilities, And Resistivities Obtained from Hall Effect Measurements from Cu$_2$O Films on Glass Annealed at Various Temperatures[a]

sample	annealing time and temperature	carrier concn (10^{15} cm^{-3})	mobility (cm^2/V·s)	Hall resistivity (Ω·cm)
1	250 °C, 1 h	1.89 ± 0.31	2.59 ± 0.23	1290
2	300 °C, 1 h	1.02 ± 0.14	8.68 ± 1.28	900
3	350 °C, 1 h	1.75 ± 0.27	7.26 ± 1.11	490
4	350 °C, 6 h	3.58 ± 0.32	12.67 ± 0.83	200
5	400 °C, 1 h	8.47 ± 0.34	6.07 ± 0.20	125

[a] Parameters of films annealed at less than 250°C could not accurately be determined.
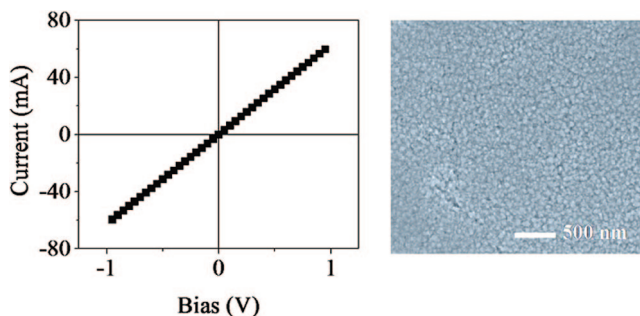
Figure 6. $J-V$ Curve of a ZnO/Cu$_2$O solar cell with no interceding TiO$_2$ layer and corresponding top-down SEM image.

Films annealed at temperatures lower than 250 °C could not be measured in the Hall apparatus because the resistance between adjacent contacts was too high.

Solar Cell Performance and Analysis. The thickness of the Cu$_2$O films in the solar cells was tracked via optical absorption. Using a combination of UV−vis absorption, profilometry, and cross-sectional SEM measurements, we have calculated the optical absorption coefficient (α) to be 3.4×10^4 cm^{-1} at a wavelength of 550 nm, which would require a micrometer thick film to have reasonable light absorption. After the ZnO NW arrays were filled with Cu$_2$O NPs to the desired height and annealed to remove surface ligands, Al contacts were evaporated onto the top of the film and the device was tested in the dark and under AM 1.5 and 1 Sun illumination. The Al contacts were used for cells annealed at 300 °C, while the Au contacts were used for cells annealed at 200 °C. For cells annealed at 300 °C, Au contacts yielded worse-performing cells. However, unlike in the case of films annealed at 200 °C, devices made using annealing temperatures of 250 °C or higher always resulted in shorted cells (Figure 6). This was true even when the Cu$_2$O film was built up to more than 10 times the height of the ZnO NW array. Top-down SEM images of the completed films showed that, while the films were rough in texture, there were no large crevices or pinholes that could lead to the evaporated Al contacts shorting to the ITO substrate underneath. The lack of metallic behavior in the Hall measurements as well as the absence of any Cu peaks in the XRD patterns would seem to preclude this as the cause of shorting as well.

It was not until a blocking layer of TiO$_2$ was deposited, via atomic layer deposition (ALD) onto the ZnO NWs before the Cu$_2$O NP deposition began, that functioning cells could be obtained. Figure 7 shows the $J-V$ curves of a solar cell made from a 500-nm long ZnO NW array, coated with 10 nm of TiO$_2$, and filled in with Cu$_2$O NPs until the film was 800 nm in height. The photovoltaic figures of merit all improve dramatically, and the efficiency rises by a factor of 50. Overall, however, the
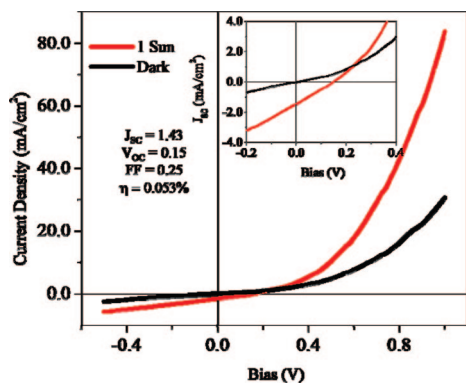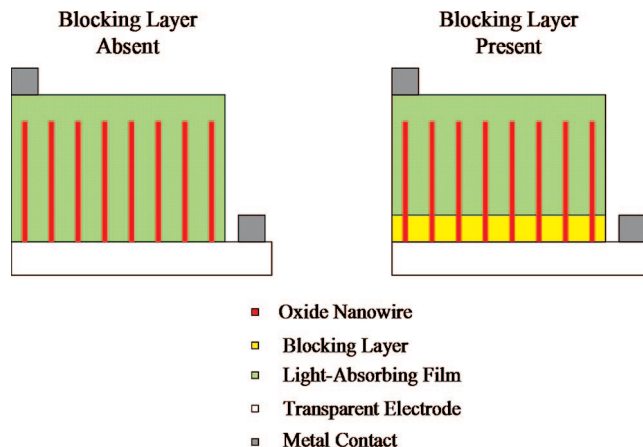
Figure 7. $J-V$ curves of a ZnO/TiO$_2$/Cu$_2$O solar cell in darkness and under 1 Sun illumination. The Cu$_2$O film was annealed at 300 °C under 500 mTorr of oxygen. The ZnO NWs are 500 nm in length, the TiO$_2$ coating layer is 10 nm thick, and the Cu$_2$O film thickness is 800 nm.

efficiency is still rather low, with average values being 0.02−0.03% and the best efficiency obtained being 0.053%. While this efficiency is quite small, it is still ∼10 times higher than that of comparably constructed thin film devices (i.e., where the ZnO NW array was replaced with an ALD ZnO film). This figure is half the efficiency of a previously reported solar cell also employing ZnO nanowires and a Cu$_2$O thin film.[23] In contrast to the present work, this solar cell employed vapor-phase methods to fabricate both the ZnO and Cu$_2$O components (vapor deposition and sputtering, respectively). The sputtered Cu$_2$O film only coated the tips of the ZnO NWs, leaving large void spaces in between the film and the transparent electrode. Although this device architecture does not take full advantage of the small interwire dimensions which could allow for greater interfacial area, it also does not appear to have the shorting problems that we report as a consequence of completely filling in the nanowire array with Cu$_2$O NPs. It was found that the minimum TiO$_2$ thickness required to obtain nonshorting devices was ∼5 nm. The peak efficiencies were obtained with a TiO$_2$ thickness of ∼10 nm, while thicker coatings of TiO$_2$ led to gradually lower efficiencies, mostly through a reduction of the short circuit current density, J_{SC}.

In a previous study involving polymer−inorganic hybrid solar cells,[24] we observed a notable increase in solar cell performance when an ALD layer of TiO$_2$ was applied to the ZnO NWs before polymer deposition. Although a similar effect is observed in this work, we believe the reason for this improvement is different in this case; for, while working cells could be obtained in the case of ZnO NW/polymer cells, we never obtained a working solar cell without TiO$_2$ when the Cu$_2$O NPs were annealed at 250 °C or higher. We believe the reason for this behavior lies in the fundamental resistances and electrical pathways in the cell.

In any solar cell, there are parasitic resistances that will contribute to the loss of photovoltaic efficiency. They can be divided into the series resistance (R_S), which includes components such as resistance through the semiconductors, as well as metal−semiconductor contact resistance, and the shunt resistance (R_{SH}), which includes the resistance of alternate electrical pathways that do not contribute to the photocurrent. In an ideal solar cell, then, R_S is zero, and R_{SH} is infinite.

(23) Hsueh, T.-J.; Hsu, C.-L.; Chang, S.-J.; Guo, P.-W.; Hsieh, J.-H.; Chen, I.-C. *Scr. Mater.* **2007**, *57*, 53.
(24) Greene, L. E.; Law, M.; Yuhas, B. D.; Yang, P. *J. Phys. Chem. C* **2007**, *111*, 18451.

Figure 8. Illustration of a nanowire-based solar cell, with and without a blocking layer between the light-absorbing material and the transparent electrode. A shunt pathway exists for the case without a blocking layer, where it is absent in the case with the blocking layer.

The major shunt pathway in our solar cell is the current passing directly through the Cu$_2$O film and bypassing the ZnO NWs entirely (Al−Cu$_2$O−ITO pathway). Using the resistivities obtained from the Hall measurements, we can approximate the expected shunt resistance using the height of the film and the area of the metal contacts. The absolute resistance, R, is related to the resistivity as follows: $R = \rho L/A$, where ρ is the resistivity in $\Omega \cdot$cm, L is the length of the conduction pathway in cm, and A is the contact area in cm^2. If we use the resistivity measured for the 300 °C annealing condition listed in Table 1, and the film and contact dimensions from the cell in Figure 7, then we obtain a resistance of 2.4 Ω. This is an exceedingly small resistance, which in fact is dwarfed by the sheet resistance of the ITO substrate (∼40−50 Ω/square). This may explain why the currents measured on the shorted devices always reflect a resistance of 40−50 Ω.

The characteristic resistance of a solar cell, R_{CH}, is defined as[2] $R_{CH} = V_{OC}/I_{SC}$. If the series resistance is much larger than or the shunt resistance is much smaller than R_{CH}, there will be major detrimental effects to the device performance. Using the values of V_{OC} and I_{SC} measured from the device in Figure 7, we find a characteristic resistance of ∼3500 Ω. This is far greater than the shunt resistance calculated for the Cu$_2$O film. Even if the film is 10 times as thick, R_{SH} would still be only ∼24 Ω, well below R_{CH}. By comparison, an earlier work[24] from our group involving a nanowire-based polymer−inorganic hybrid cell uses the same cell geometry but employs a polymer that is far more resistive than the Cu$_2$O film. In this scenario, the shunt pathway still exists but is likely less of a concern owing to the greater value of R_{SH}.

It is likely, then, that the act of coating TiO$_2$ on the ZnO NW array forms a barrier at the base of the array (as well as on the wire sidewalls) that acts to sufficiently increase R_{SH} such that working cells can be obtained. Of course, this barrier will also affect carrier extraction, but the similarity in band positions between ZnO and TiO$_2$ somewhat compensates for this.

The problem of the low shunt resistance has rather profound consequences for a solar cell constructed from a nanowire array. Figure 8 illustrates two similarly designed nanowire-based solar cells, with the difference being the presence of a blocking layer between the light absorbing material and the transparent electrode. The interwire spacing and necessary exciton diffusion length are similar in each case. However, without the blocking

layer present, filling in the nanowire array with the second, light-absorbing (and conductive) component will introduce a shunt pathway. A solar cell with a nanowire array synthesized directly on an electrode without a buffer layer, such as in our ZnO NW synthesis, will lead to this scenario. If the resistivity of the filling material is rather large, as in the case of a polymer, then R_{SH} will be comparatively larger and may not have an overly detrimental effect on photovoltaic performance. However, as the resistivity decreases, so will R_{SH}. We thus see that while higher-conductivity materials are desirable to facilitate charge conduction once the exciton is split, there will be an opposing, deleterious effect manifested in the lower shunt resistance.

Conversely, if a relatively nonconductive blocking layer is present, the previously described shunt pathway no longer exists, because the light-absorbing material can no longer be in direct contact with the back electrode. This scenario could be achieved by selectively depositing the blocking layer in between the nanowires (Figure 8).

Finally, we performed stability tests of our ZnO/TiO$_2$/Cu$_2$O cells. $J-V$ characteristics of two devices were tested and then stored in ambient conditions for 6 months and retested. Very little degradation is observed in this time frame, which is an encouraging result, given that a major purported advantage of an all-oxide solar cell is its long-term environmental stability. It is probable, then, that if the overall efficiency of such cells could be increased, the enhanced performance would persist for many months thereafter.

Conclusions

The all-oxide nanowire-based solar cell represents, in many ways, an ideal design for a solar cell. The use of a vertically aligned nanowire array eliminates the problem of exciton diffusion versus light absorption by allowing the light to be absorbed in the vertical direction while allowing exciton extraction in the orthogonal direction. In addition, the use of inexpensive, environmentally benign, and stable oxide materials

suggests that a device constructed in this manner could have an excellent working lifetime at a fraction of the cost of existing solar cells.

Our two major and unexpected findings, which likely prevented our cells from attaining efficiencies greater than 0.05%, could have a significant impact on solution-based nanowire solar cells in general. Our observation of an unexpected evolution of the Cu$_2$O NP films suggests a very strong dependence of film phase and morphology, and ultimately device performance, on the nanoparticle film process conditions. Such film processing of the nanoparticles will be a major issue in the construction of photovoltaic devices. This is especially true in the case of transition metal oxides and sulfides, such as Cu$_2$S and FeS$_2$, which have been demonstrated as ideal candidates for use in solar cells for many of the same reasons cited for Cu$_2$O. Second, our observation of the very important dependence of the shunt resistance on the photovoltaic performance is widely applicable to any nanowire solar cell constructed with the nanowire array in direct contact with one electrode. Filling the arrays with a moderately conductive material, such as Cu$_2$O, creates a situation where the shunt resistance is quite low simply by virtue of the short distance required to complete the shunt pathway. The bottom-up synthesis of the oriented nanowire array is one of the most elegant and versatile architectures for constructing practical nanoscale devices. However, it also introduces other complicating factors which must be addressed separately to fully realize effective nanowire-based photovoltaic devices.